Int. J. Electrochem. Sci., 10 **(2015)** 5673 - 5693

International Journal of
ELECTROCHEMICAL
SCIENCE
www.electrochemsci.org

Corrosion Behavior of Carbon Steel in LiBr in Comparison to NaCl Solutions under Controlled Hydrodynamic Conditions

Alvaro Soliz * *and Luis Cáceres.*

CICITEM, Centro de Investigación Científico y Tecnológico para la Minería, Departamento de Ingeniería Química y Procesos de Minerales, Universidad de Antofagasta, Av. Angamos 601, Antofagasta, Chile
*E-mail: alvaro.soliz@uantof.cl

Received: 9 February 2015 / *Accepted:* 3 April 2015 / *Published:* 27 May 2015

The corrosion behavior of carbon steel AISI 1020 in LiBr in comparison with NaCl aqueous solutions were studied from polarization curve measurements in a rotating disk electrode under a combination of salt concentration and rotation speed of the electrode. Assuming the occurrence of hydrogen evolution and oxygen reduction as the cathodic counterparts of the iron oxidation under a predetermined kinetic model, the corresponding kinetic parameters were obtained applying a numerical method to experimental data. It was found that, despite of the close similarities observed between corrosion behavior of carbon steel in LiBr, NaCl and the mixture LiBr+NaCl, there are distinct differences in kinetics for partial reactions. Some relevant aspects are the significant differences for iron oxidation and hydrogen evolution in the kinetics parameters that indicates higher kinetic rate for LiBr in comparison with NaCl solutions. This can be related with morphological attributes of the pits. For oxygen reduction the fluid dynamics regime and transport properties of the electrolyte of each salt solution are the main factors affecting the oxygen kinetic behavior.

Keywords: Carbon steel; Kinetic parameters; Halide ions; Mixed potential

1. INTRODUCTION

Corrosion is defined as the destructive attack of a metal by reaction with its environment [1, 2]. In addition to selecting the type of metal, any fundamental approach of the corrosion must involve considerations about the nature of the environment and the metal/environment interphase, such as the concentration of aggressive species in solution, fluid motion, the kinetic of metal oxidation and the reduction of the species at the metallic surface [1].

Lithium bromide is one of the most widely used absorbents in the industry due at the favorable thermo-physics properties, such as its high solution enthalpy of ΔHs= -49 KJ mol^{-1}, in comparison to NaCl or LiCl with solution enthalpies of ΔHs= 4 KJ mol^{-1} and ΔHs= -37 KJ mol^{-1}, respectively [3-5]. Like sodium chloride, the lithium bromide solutions can cause serious corrosion problems on the steel structures and machine components [6]. Previous studies on the corrosion behavior of steel in halide solution cover general aspects related to anodic dissolution, transition from active to passive region, pitting potential measurements, current oscillations during pitting formation and kinetics of passive film formation and breakdown [6-8]. Conflicting conclusions are for a relative pitting potential and breakdown, while a report indicates no breakdown potential difference in the presence of different halides, another report concludes a significant pitting potential variation between halides.

Because of its corrosion vulnerability of steels to salt containing solutions under near neutral, oxygenated or aerated conditions, the deployment of preventive measures to mitigate corrosion becomes in many cases a necessity to minimize high replacement costs. In order to be effective, these measures require an accurate knowledge of the corrosion behavior of carbon steel under varied conditions [9-12].

A general assumption for corrosion studies of steel in aqueous solutions is that hydrogen evolution and/or oxygen reduction are the main counterpart reactions for iron oxidation. The role of halide ions in the corrosion process is through particular effects such as physicochemical transport properties and charge interactions that influence the kinetic mechanism of partial reactions. Given the industrial importance of corrosion at industrial scale and the widespread presence of chlorides in water, most of the corrosion studies have been done in chloride containing water. Particularly for highly concentrated chloride solutions, carbon steel can be mainly affected by localized attack (pitting corrosion), which is a form of damage caused by a combined effect of high content of aggressive anions and fluid motion [6, 9, 13, 14]. For the purpose of corrosion modelling it is assumed that localized corrosion taking place as distributed pits is equivalent to a uniform corrosion throughout the exposed surface. This applies not only for iron oxidation but also for the counterpart cathodic reactions. In this regards, the corrosion modelling and the determination kinetic parameters are commonly performed using the extrapolation Tafel method, in which the graphical representation of the logarithm of the current density (log |i|) versus the electrode potential (E) shows a linear relation in the anodic and cathodic domain. From these graphics, the straight lines for both domains are extrapolated linearly and their intersection point defines the corrosion potential and current density [1, 13, 15]. For the application of this method, it is necessary that both domains, anodic and cathodic, must be under an activation control showing a well-defined Tafel region [13, 15]. Moreover, when the polarization curves do not shows a sufficient Tafel region, as to use the extrapolation method [16-19], the polarization curves can be analyzed through of a numerical adjustment using the superposition model and the mixed potential theory proposed by Warner and Traud [2, 20, 21].

In this work, we study the corrosion behavior of carbon steel AISI 1020 immersed in diluted and concentrated solutions of LiBr in comparison with NaCl solutions, using potentiodynamic measurements in a rotating disk electrode under varied conditions of halide concentration, rotation rates, and presence and absence of dissolved oxygen concentration. Applying the mixed potential theory for the corrosion process, the electrochemical corrosion parameters for all partial corrosion

reactions were determined for all conditions studied. From this information detailed behavior for each partial reaction and global trends were discussed.

2. EXPERIMENTAL

Test unbuffered NaCl and LiBr solutions at concentration of 0.5, 1 and 2 mol L^{-1} respectively were prepared using analytical-grade reagent and distilled water. Also, to investigate the combined effect of NaCl and LiBr on the corrosion behavior, solutions containing a NaCl-LiBr in the molar ratio of 1:1 were prepared to give a total salt concentration of 0.5, 1 and 2 mol L^{-1}. Before each measurement, the solutions were oxygenated with high purity air by bubbling for a period of 15 min at a room temperature of 21 °C. The air flow into the solutions was maintained till the end of the experiences. Physical properties of the electrolyte solutions were calculated using predictive correlations [22-25]. For the mixed solution containing NaCl and LiBr the physical properties were approximated by the weighted average based on its concentrations. Values of density (ρ), kinematic viscosity (ν), oxygen diffusivity (D), and bulk oxygen dissolved concentration ($C_{b,O2}$) are tabulated in Table 1 for each test solution studied. An optical dissolved oxygen meter type ORION 3-Star Plus was used for the measurements of the dissolved oxygen concentration in solution. In order to determine the oxygen influence on the electrochemical measurements, additional experiences were performed under deaerated conditions, in which the dissolved oxygen in solution was purged by bubbling with high purity nitrogen for 20 min.

Table 1. Physical properties of the NaCl and LiBr electrolyte solutions at 21 °C

	ρ [17, 19] Kg m^{-3}	$10^7\nu$ [17, 19] m^2 s^{-1}	$10^9 D_{O2}$ [18, 20] m^2 s^{-1}	$C_{b,O2}$ mol m^{-3}	Predicted Levich slope	Experimental Levich slope
NaCl, mol L^{-1}						
0.5	1018.2	9.18	2.03	0.21	0.82	0.71
1.0	1036.4	9.41	1.93	0.19	0.71	0.68
2.0	1072.3	10.1	1.88	0.14	0.51	0.49
LiBr, mol L^{-1}						
0.5	1030	8.98	1.99	0.23	0.89	0.83
1.0	1076.4	9.96	1.70	0.22	0.75	0.69
2.0	1124.7	9.99	1.65	0.19	0.63	0.58
xNaCl+xLiBr, mol L^{-1}						
x=0.25	1012.7	9.0	2.12	0.24	0.96	0.85
x=0.5	1024.1	9.08	2.01	0.22	0.85	0.79
x=1.0	1056.4	9.70	1.82	0.20	0.72	0.59

Electrochemical measurements were performed using a conventional three-electrode glass cell with a rotating disc electrode (RDE) system. The working electrodes (4 mm diameter and 10 mm length) were made from small cylindrical carbon steel AISI 1020 bars whose chemical composition was wt%: 0.2 C, 0.6 Mn, 98.5 Fe and traces of S, Si, Cu, Ni, Cr, Sn, P and Mo. The metallic specimen were inserted into a plastic rod (8 mm diameter and 20 mm of length) with appropriate perforations and sealed applying resin adhesive, so that only the bottom planar surface area (12.57 mm^2) was exposed to the test solution. Prior to each experiment, the working electrodes were mechanically polished using 1200-grit SiC polishing paper, washed with ethanol in an ultrasonic bath, and finally rinsed with distilled water. Spiral platinum and an Ag/AgCl (sat. KCl) were used as counter and reference electrodes respectively. An EPSILON potentiostat/galvanostat (Bas Inc. USA) model BAS100 B/W provided with a rotating electrode interface BAS/RDE-1 was used as electrochemical interface. Experiments were carried out for a range of rotation speed between 1500 and 6863 rpm. Linear sweep voltammetry measurements were performed by sweeping the potential in positive direction from -950 mV to -50 mV versus the standard hydrogen electrode (SHE) at a potential scan rate of 1 mV s^{-1} which is assumed to produce a steady-state condition [1]. The starting potential and the sweep direction ensure that the measurements can be performed on a free-oxides surface, thereby controlling the excessive generation of hydrogen microbubbles at the specimen. The morphological inspections of the corroding surface were observed using a LEO 1420 VP scanning electron microscopy (SEM), and an optical microscope Olympus BX 41M.

3. RESULTS AND DISCUSSION

3.1. Polarization curves in aerated and deaerated solutions

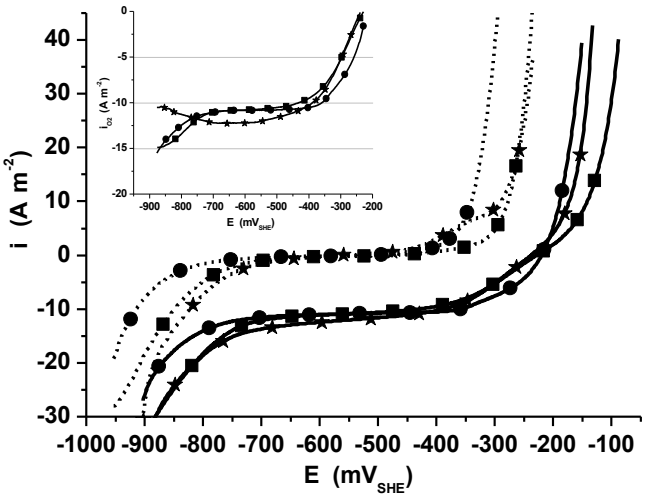

Figure 1. Experimental polarization curves for carbon steel in aerated (continuous line) and deaerated (dotted line) 1 mol L^{-1} NaCl (circle), 1 mol L^{-1} LiBr (square) and 0.5 mol L^{-1} NaCl + 0.5 mol L^{-1} LiBr (stars) solutions. Scan rate of 1 mV s^{-1}, and rotation speed of 2500 rpm. Inset: Difference between aerated and deaerated experimental data.

Neglecting the occurrence of any electrochemical partial reaction other than oxygen reduction, hydrogen evolution and iron reduction in a metal immersed in an aqueous salt solution, it can be stated that a partial polarization curve for oxygen reduction reaction can be visualized by superimposing of the experimental aerated and deaerated polarization curves. Under this consideration, the Fig. 1 shows potentiodynamic measurements for carbon steel immersed in aerated and deaerated NaCl and LiBr solutions. In the figure it is seen that the experimental polarization curves exhibits similar shapes and symmetry. According to the mixed potential theory, these shapes can be synthesized as a superimposition of the partial reactions that occurs in the corrosion process [26-28].

The partial reactions taking place during the corrosion of carbon steel are:

$$2H_2O+2e^- \rightarrow H_{2\,(g)}+ 2OH^-_{(aq)} \quad (1)$$

$$O_{2\,(g)}+2H_2O+ 4e^- \rightarrow 4OH^-_{(aq)} \quad (2)$$

$$Fe \rightarrow Fe^{+2}_{(aq)} + 2e^- \quad (3)$$

The kinetics expressions for the partial cathodic and anodic reactions are:

The cathodic reactions:

$$i_{H2}=i_{0,H2}\exp\left(\frac{2.303\left(E-E_{eq,H2}\right)}{b_{H2}}\right) \quad (4)$$

$$i_{O2}=i_{0,O2}\exp\left(\frac{2.303\left(E-E_{eq,O2}\right)}{b_{O2}}\right)\left(1-\frac{i_{O2}}{i_{l,O2}}\right)^m \quad (5)$$

The anodic reaction:

$$i_{Fe}=i_{0,Fe}\exp\left(\frac{2.303\left(E-E_{eq,Fe}\right)}{b_{Fe}}\right) \quad (6)$$

where, $i_{0,j}$ is the exchange current density, b_j is the Tafel slope, $E_{eq,j}$ is the equilibrium potentials, with subscripts designating (j) of oxygen reduction (O_2), hydrogen evolution (H_2) and iron oxidation (Fe), respectively, $i_{l,O2}$ is the oxygen limiting current density, and m is the kinetic order for the oxygen reduction reaction (ORR). The equilibrium potentials for the reaction (1)-(3) were determined using the Nernst equation:

$$E_{eq,O2}=E^0_{O2}-\frac{0.0584}{4}(4pH-\log(P_{O2})) \quad (7)$$

$$E_{eq,H2}=E^0_{H2}-\frac{0.0584}{2}(2pH-\log(P_{H2})) \quad (8)$$

$$E_{eq,Fe}=E^0_{Fe}+\frac{0.0584}{2}\left(\log\left(C_{Fe^{+2}}\right)\right) \quad (9)$$

where, E^0_j is the standard equilibrium potential for oxygen reduction, hydrogen evolution and iron oxidation respectively, P_{O2} and P_{H2} are the partial pressures for oxygen and hydrogen, and C_{Fe}^{+2} is

the ferrous iron concentration. A ferrous iron concentration value of $1x10^{-6}$ mol L^{-1} was assumed for E_{eqFe} calculation as suggests Bockris [29].

The absence of a planar plateau in the anodic and cathodic domain of the polarization curves for deaerated solutions (Fig. 1) indicates that electrochemical reactions are under an activation control, which can be identified from the Tafel slope in Evans plots. It condition can be due at the sufficient water molecules available on the metallic surface for its reduction reaction [30].

For aerated solutions, the presence of a distinctive cathodic plateau in the polarization curves is fully compatible with the kinetic expression given by Eq. (5) in the potential range between -700 mV_{SHE} and -400 mV_{SHE} [9, 27, 31, 32]. On the other hand, the corrosion potential shifting toward more positive potentials exhibited for aerated solutions, in comparison with deaerated solutions, can be easily visualized in terms of the mixed potential theory considering that the aerobic polarization curve is nearly equivalent to a superimposition between a partial cathodic oxygen reduction current density and a deaerated polarization curve.

The difference between the experimental aerobic and anaerobic polarization curves is shown as an insert in Fig. 1. In the cathodic side of this curve, the NaCl deviation toward more negative values in comparison with LiBr suggests a different kinetic rate for each case or a synergistic interaction between oxygen reduction and hydrogen evolution reactions. This interaction can be originated from local increases of pH which takes place from the reduction reactions (1) and (2). This increase in pH should generate a decrease in the equilibrium potential values of Eqs. (7) and (8), that subsequently alter the kinetics rate through changes induced in the overpotential values of Eqs. (4) and (5). For the case of hydrogen evolution reaction (assuming that the exchange current density value remains unaltered), an increase of current density is expected as a result of a pH increase. Given the significant larger current densities for aerated in comparison with deaerated solutions, then a significant larger increase in local pH is expected for aerated solutions. This is compatible with deviations shown in the cathodic side of the difference between experimental curves shown in Fig. 1.

3.2. Rotation speed influence on polarization curves

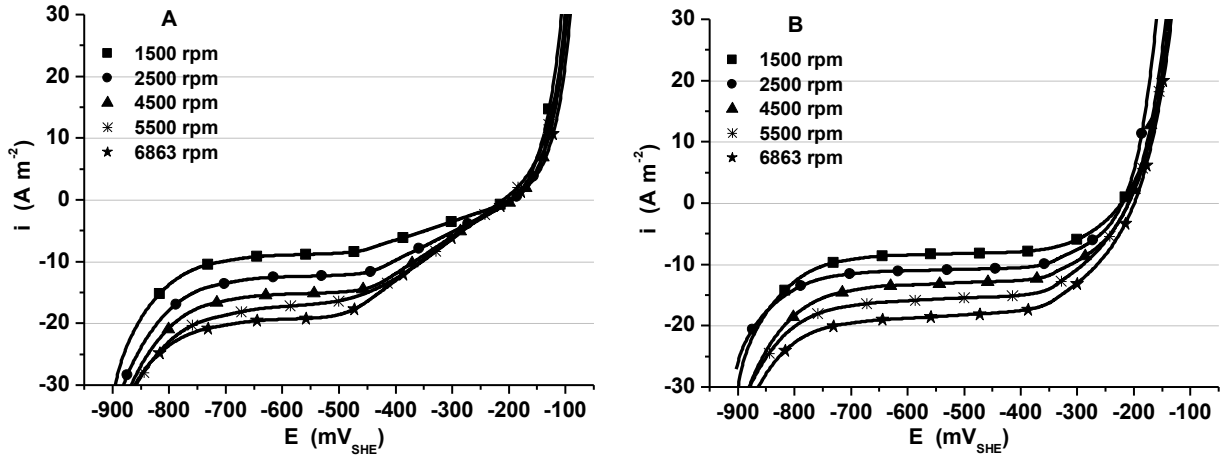

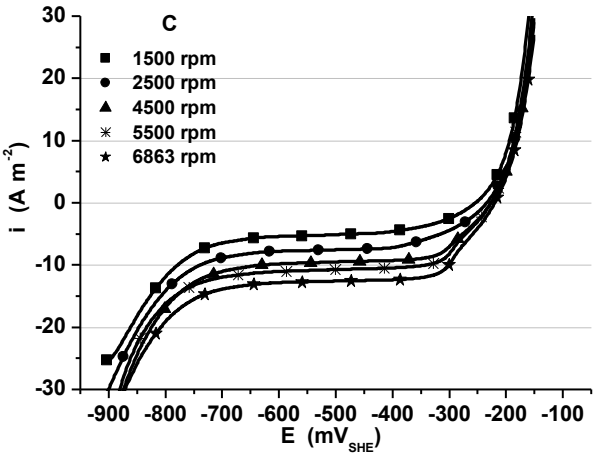

Figure 2. Influence of the rotation speed on polarization curves for carbon steel electrodes in aerated (A) 0.5, (B) 1.0 and (C) 2.0 mol L^{-1} NaCl solutions. Scan rate 1 mV s^{-1}.

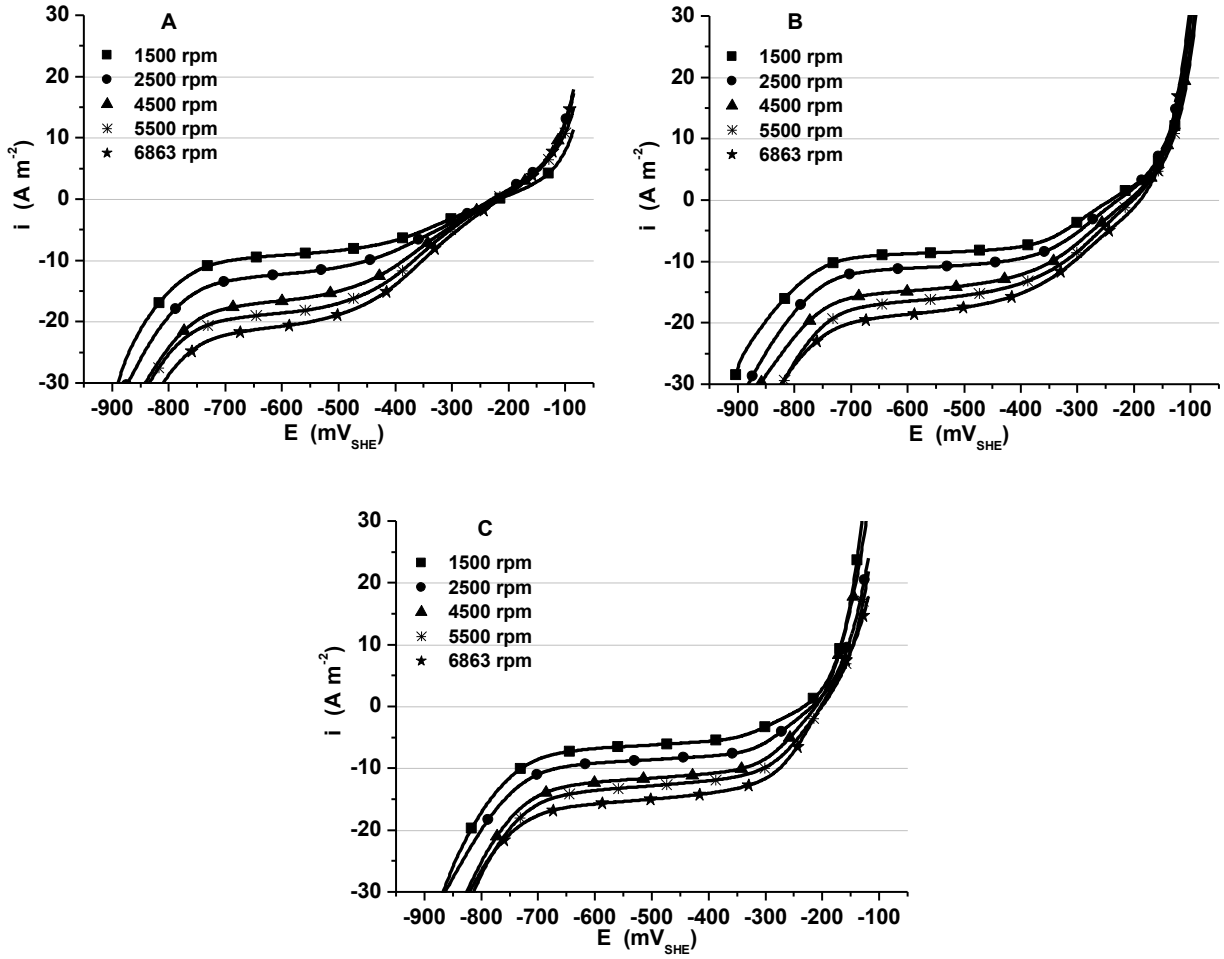

Figure 3. Influence of the rotation speed on polarization curves for carbon steel electrodes in aerated (A) 0.5, (B) 1.0 and (C) 2.0 mol L^{-1} LiBr solutions. Scan rate 1 mV s^{-1}.

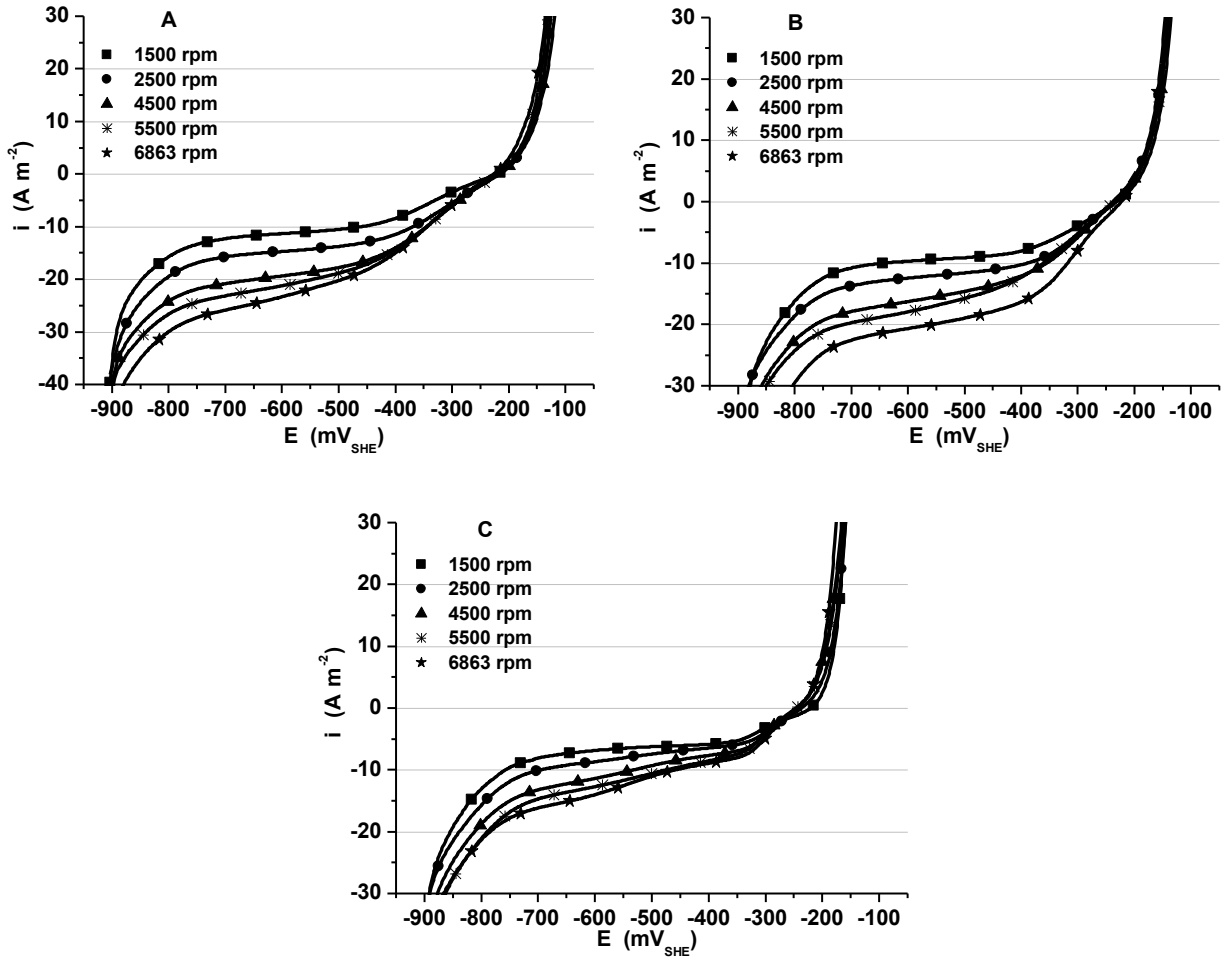

Figure 4. Influence of the rotation speed on polarization curves for carbon steel electrodes in aerated (A) 0.25 mol L^{-1} LiBr + 0.25 mol L^{-1} NaCl, (B) 0.5 mol L^{-1} LiBr + 0.5 mol L^{-1} NaCl, and (C) 1.0 mol L^{-1} LiBr + 1.0 mol L^{-1} NaCl solutions. Scan rate 1 mV s^{-1}.

Figs. 2-4 presents typical polarization curves for carbon steel electrodes immersed in aerated individuals NaCl and LiBr solutions and a mixture NaCl+LiBr at various rotation speeds. No visual difference can be observed between different polarization curves at every concentration whose shapes and trends that are in agreement with previous investigations concerning the corrosion studies of carbon steel in NaCl solution [9, 20]. The main feature observed in all group of experiments an every salt concentration is that the planar plateau, which is mainly originated from the limiting current density for ORR, shows a notorious increase in magnitude with increasing rotation speed. This effect is directly related to the decreasing trend of the diffusion layer thickness with increasing rotation speed [13, 33-35]. In principle the planar plateau should persist with increasing potentials while the dissolved oxygen concentration has a null value at the metal surface. The gradual decrease of the planar plateau that occur at potentials more positive than -400 mV_{SHE}, is due either to a ORR kinetic change from diffusion to a mixed charge transfer and mass transfer controlled mechanism, and/or the superimposition of the partial polarization curve for iron oxidation [9, 33]. In contrast with the cathodic response to a rotation speed, the anodic domain exhibits a low sensitivity to rotation speed

changes. Evidence of pitting formation on the specimen surface was confirmed in all experiments. Some pits showed rust trails indicating a corrosion product from inside the pits that was exposed to advective flow generated from the rotating specimen. According to this evidence the moderate effect of rotation speed observed on the anodic branch could be attributed to the random character of pitting corrosion that in turn could be affected by mechanism of lateral dispersion of corrosion products from inside the pits (more details in next section 3.6).

3.3. Concentration influence on the polarization curves

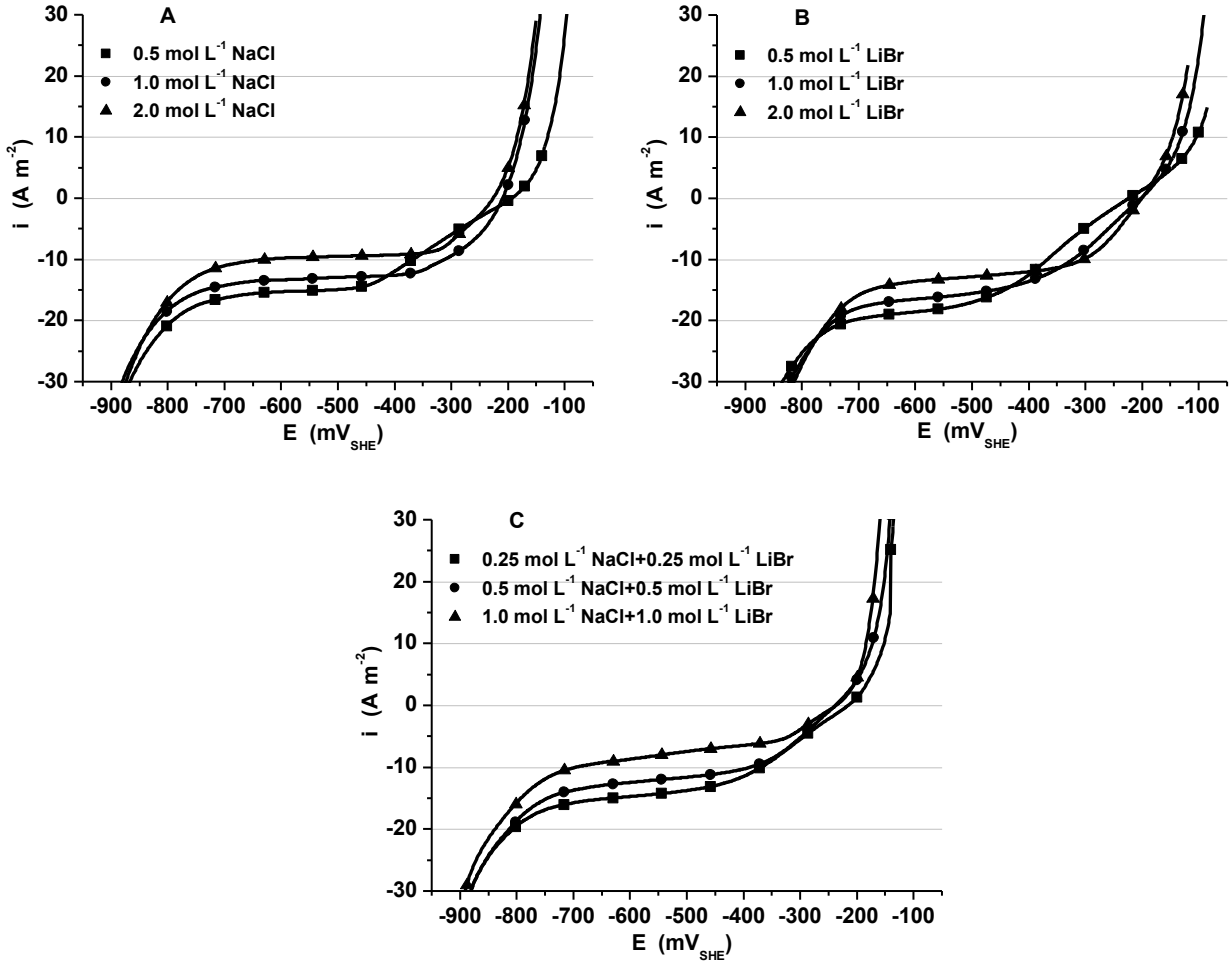

Figure 5. Polarization curves for carbon steel immersed in different concentrations of aerated (A) NaCl, (B) LiBr, and (C) NaCl+LiBr solutions at 4500 rpm, 5500 rpm and 2500 rpm respectively. Scan rate 1 mV s^{-1}.

Representative polarization curves for carbon steel immersed in different concentrations of individual NaCl and LiBr solutions and a mixture NaCl+LiBr solutions are shown in Fig. 5 for a fixed rotation speed. Similar curve shapes of the polarization curves were observed for all rotation speed

studied. Irrespective of the type of solution, the magnitude of the cathodic plateau that represents the limiting current density of the ORR shows a decreasing trend with the increasing solution concentration. These changes are related to the concentration dependency of the physical properties with concentration solution. This is the case for the oxygen diffusivity and solubility that decreases with an increase in solution concentration; in contrast the viscosity and density increase with solution concentration (Table 1). In terms of potential ranges, an increase of salt concentration reduces the region of the mixed charge transfer for the ORR, leading to an increase in the potential range for the oxygen limiting current density. For instance, in 0.5 mol L^{-1} NaCl solutions, it is seen that the mass transfer control region ranged from -700 mV_{SHE} to -500 mV_{SHE}, while that for concentrated solutions 2 mol L^{-1} NaCl the mass transfer control region ranged from -700 mV_{SHE} -320 mV_{SHE}. Similar behaviors were observed for the case of LiBr solutions and the mixed NaCl+LiBr solutions. These changes in kinetics mechanism are associated to the kinetic parameter dependency with the salt concentration, such as the Tafel slope and exchanges current density for each partial reaction [13].

3.4. Kinetic parameters and kinetic behavior of partial electrochemical reactions

Generally the determination of electrochemical and corrosion parameters from experimental polarization curves are carried out by applying the Tafel extrapolation method or the mixed potential theory [9, 12, 18, 20]. The requirements to use each method are described in literature [1, 13, 15, 21]. In the present study, as is shown in Figs. 2-5, the cathodic zone of the experimental polarization curves does not exhibit a very well-defined linear Tafel region, where current density is controlled by a mixed kinetic and mass transfer. For this reason the use of the graphical Tafel extrapolation method may lead erroneous readings. Then, the electrochemical and corrosion parameters are more conveniently determined by numerical fitting using the principle the mixed potential theory proposed by Wagner and Traud [20, 21]. This principle considers that the total current density is an algebraic contribution of the anodic and cathodic partial current densities [2, 13, 18, 20, 21].

As was discussed previously, iron oxidation, oxygen reduction and hydrogen evolution reactions are the main electrochemical partial reactions involved in the corrosion of carbon steel in aerated solutions. Then the total current density i can be written by:

$$i=i_{Fe}+i_{O2}+i_{H2} \quad (10)$$

where, i_{Fe}, i_{O2}, i_{H2} are the partial current densities for iron oxidation, oxygen reduction and hydrogen evolution reactions, respectively.

Considering a charge transfer control for the iron oxidation and hydrogen evolution reactions and a mixed charge transfer and mass transfer control for the ORR, the partial reactions can be modeled using the Eqs. (4)-(6). A first order kinetic model is considered for the ORR [9, 27, 34]. The root mean square error was used as index of convergence. Corrosion potentials E_{corr} and corrosion current densities i_{corr} were determined from Eq. (10) for a null total current density i=0 A m^{-2}.

Table 2. Electrochemical and corrosion parameters for carbon steel corrosion immersed in aerated NaCl solutions at different rotation speeds.

		Iron oxidation		**Hydrogen evolution**		**Oxygen reduction**				
NaCl, mol L^{-1}	w, rpm	b_{Fe}, mV dec^{-1}	$10^5\, i_{0Fe}$, A m^{-2}	b_{H2}, mV dec^{-1}	$10^3\, i_{0H2}$, A m^{-2}	b_{O2}, mV dec^{-1}	$10^{10}\, i_{0O2}$, A m^{-2}	i_{lO2}, A m^{-2}	E_{corr}, mV_{SHE}	i_{corr}, A m^{-2}
0.5	1500	60	0.01	-136	-3.09	-154	-1565.31	-9.08	-199	1.10
	2500	68	0.08	-131	-2.63	-137	-285.84	-12.61	-193	1.30
	4500	73	0.25	-122	-1.45	-134	-189.56	-15.56	-194	1.40
	5500	88	3.65	-165	-13.84	-137	-315.39	-17.15	-205	1.78
	6863	92	4.17	-128	-1.50	-146	-860.21	-19.83	-197	1.55
	Av.	**76**	**1.63**	**-137**	**-4.50**	**-141**	**-643.26**	**-14.85**	**-198**	**1.43**
1	1500	91	16.69	-153	-8.86	-108	-7.18	-8.20	-222	3.34
	2500	65	0.36	-152	-5.87	-117	-46.16	-10.88	-221	4.04
	4500	73	1.15	-163	-15.52	-115	-47.67	-12.99	-209	4.45
	5500	82	4.63	-157	-10.58	-108	-10.55	-15.62	-209	4.33
	6863	83	5.17	-152	-8.16	-128	-569.59	-18.52	-199	5.73
	Av.	**79**	**5.60**	**-156**	**-9.80**	**-115**	**-136.23**	**-13.24**	**-212**	**4.38**
2	1500	74	2.03	-163	-23.55	-108	-2.51	-5.02	-253	1.66
	2500	77	2.62	-159	-19.74	-114	-17.97	-7.50	-235	2.47
	4500	74	1.72	-161	-24.13	-77	-0.0008	-9.41	-228	2.77
	5500	71	0.96	-152	-13.38	-73	-0.0001	-10.72	-228	2.76
	6863	74	1.45	-148	-12.75	-73	-0.0001	-12.56	-222	3.00
	Av.	**74**	**1.75**	**-157**	**-18.71**	**-89**	**-4.10**	**-9.04**	**-233**	**2.53**

Table 3. Electrochemical and corrosion parameters for carbon steel corrosion immersed in aerated LiBr solutions at different rotation speeds.

		Iron oxidation		**Hydrogen evolution**		**Oxygen reduction**				
LiBr, mol L^{-1}	w, rpm	b_{Fe}, mV dec^{-1}	$10^5\, i_{0Fe}$, A m^{-2}	b_{H2}, mV dec^{-1}	$10^3\, i_{0H2}$, A m^{-2}	b_{O2}, mV dec^{-1}	$10^{10}\, i_{0O2}$, A m^{-2}	i_{lO2}, A m^{-2}	E_{corr}, mV_{SHE}	i_{corr}, A m^{-2}
0.5	1500	139	146.24	-161	-20.79	-136	-291.38	-8.80	-215	1.13
	2500	132	163.98	-166	-28.64	-141	-554.70	-11.85	-224	1.50
	4500	141	263.48	-166	-30.85	-141	-620.58	-16.25	-222	1.66
	5500	168	889.33	-148	-15.88	-140	-683.34	-18.51	-223	1.95
	6863	149	404.53	-156	-22.32	-144	-1303.29	-20.60	-213	2.02
	Av.	**146**	**373.51**	**-159**	**-23.69**	**-140**	**-690.66**	**-15.20**	**-219**	**1.65**

1	1500	123	117.97	-183	-92.38	-84	-0.02	-8.16	-241	1.33
	2500	108	41.09	-175	-96.61	-97	-1.15	-10.43	-226	1.67
	4500	101	18.95	-172	-93.30	-122	-304.47	-14.13	-208	2.14
	5500	103	22.39	-166	-81.98	-126	-658.83	-15.72	-199	2.42
	6863	86	3.41	-160	-73.37	-149	-14740.23	-18.16	-189	3.05
	Av.	**104**	**40.76**	**-171**	**-87.53**	**-116**	**-3140.94**	**-13.32**	**-213**	**2.12**
2	1500	80	2.49	-166	-176.58	-112	-61.76	-6.10	-232	1.60
	2500	98	21.52	-162	-169.68	-101	-13.87	-8.44	-218	2.39
	4500	90	11.19	-160	-196.24	-104	-42.83	-11.39	-212	3.50
	5500	105	39.97	-156	-187.85	-102	-38.15	-12.61	-199	3.57
	6863	119	126.28	-180	-291.64	-86	-0.86	-14.54	-201	3.89
	Av.	**98**	**40.29**	**-165**	**-204.40**	**-101**	**-31.49**	**-10.62**	**-212**	**2.99**

Table 4. Electrochemical and corrosion parameters for carbon steel corrosion immersed in aerated xNaCl + xLiBr solutions at different rotation speeds. x=0.25 mol L^{-1}, 0.5 mol L^{-1} and 1.0 mol L^{-1}.

		Iron oxidation		**Hydrogen evolution**		**Oxygen reduction**				
x, mol L^{-1}	w, rpm	b_{Fe}, mV dec^{-1}	$10^5\, i_{0Fe}$, A m^{-2}	b_{H2}, mV dec^{-1}	$10^3\, i_{0H2}$, A m^{-2}	b_{O2}, mV dec^{-1}	$10^{10}\, i_{0O2}$, A m^{-2}	i_{lO2}, A m^{-2}	E_{corr}, mV_{SHE}	i_{corr}, A m^{-2}
0.25	1500	68	0.17	-167	-18.26	-122	-28.42	-11.06	-223	1.09
	2500	78	1.17	-172	-23.64	-126	-91.06	-14.35	-215	1.70
	4500	77	1.09	-181	-31.06	-133	-270.67	-19.13	-215	1.88
	5500	74	0.74	-206	-66.75	-142	-904.37	-20.88	-216	2.01
	6863	83	4.63	-212	-91.10	-150	-2498.60	-23.11	-225	2.42
	Av.	**76**	**1.56**	**-188**	**-46.16**	**-135**	**-758.62**	**-17.71**	**-219**	**1.82**
0.5	1500	68	0.28	-166	-28.97	-103	-0.88	-9.18	-229	1.24
	2500	80	2.92	-192	-60.80	-97	-0.26	-11.61	-235	1.78
	4500	79	2.71	-224	-136.14	-119	-34.71	-15.00	-229	2.09
	5500	81	3.57	-232	-151.07	-137	-465.23	-16.84	-229	2.16
	6863	70	0.61	-246	-247.79	-105	-2.47	-18.80	-223	2.27
	Av.	**76**	**2.02**	**-212**	**-124.95**	**-112**	**-100.71**	**-14.28**	**-229**	**1.91**
1.0	1500	39	0.00001	-179	-49.51	-85	-0.01	-6.22	-222	0.78
	2500	55	0.02	-212	-128.34	-100	-0.61	-7.35	-233	1.36
	4500	56	0.04	-234	-215.77	-125	-83.06	-9.59	-238	1.79
	5500	64	0.25	-244	-283.62	-122	-53.75	-10.66	-240	1.90
	6863	50	0.005	-263	-352.33	-146	-1625.91	-11.74	-234	2.17
	Av.	**53**	**0.06**	**-226**	**-205.91**	**-116**	**-352.67**	**-9.11**	**-223**	**1.60**

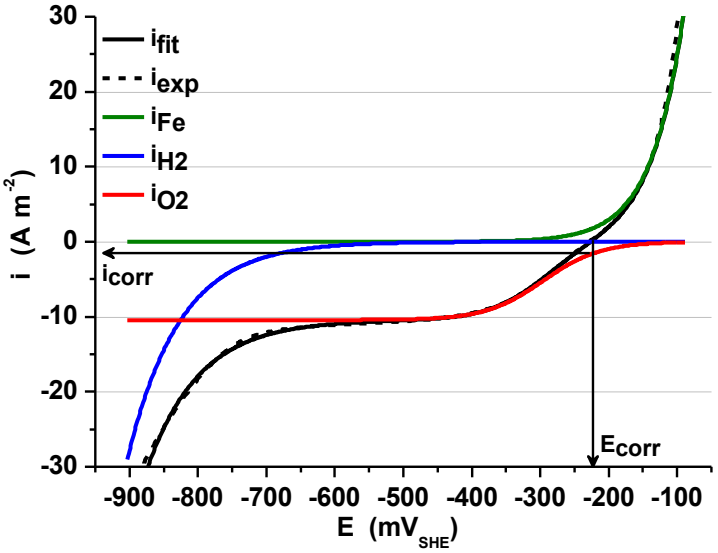

Figure 6. Experimental and fitted polarization curves for carbon steel in aerated 1 mol L^{-1} LiBr solution at 2500 rpm. Corrosion parameters determination and synthesis of the partial polarization curves using the superposition model and the mixed potential theory.

Tables 2-4 resumes the rotation speed influence on the electrochemical parameters values for the partial reactions involved in the corrosion process of carbon steel immersed in NaCl, LiBr and the mixture NaCl+LiBr solutions, respectively. Fig. 6 shows the relationship between experimental and fitted polarization curves, and synthesized partial polarization curves which were constructed using Eqs. (4)–(6) and Eq. (10).

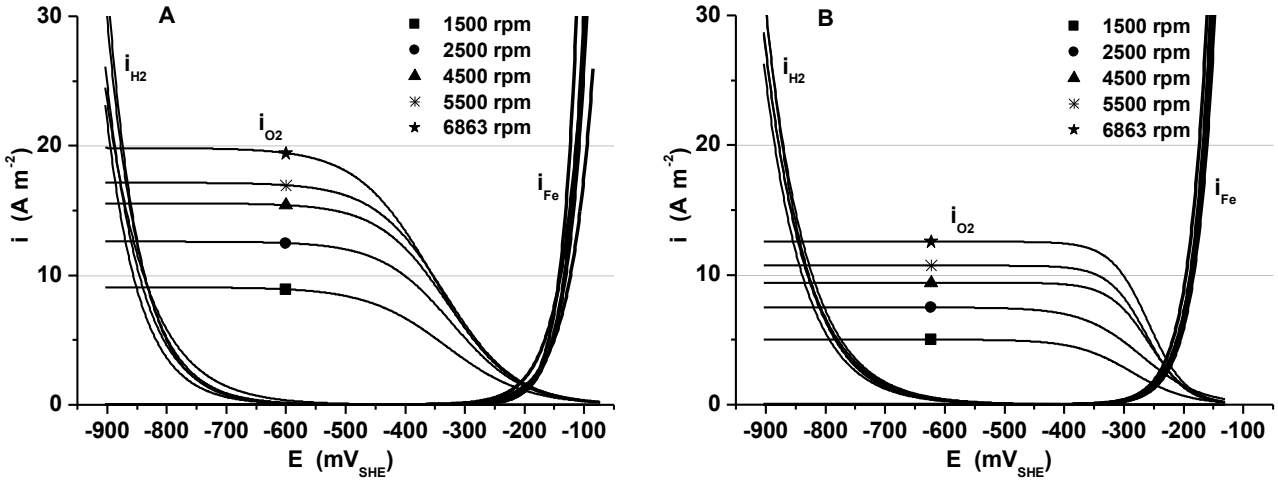

Figure 7. Rotation speed influence on partial polarization curves for anodic and cathodic sub-processes at concentrations of (A) 0.5 mol L^{-1} and (B) 2 mol L^{-1} NaCl solutions.

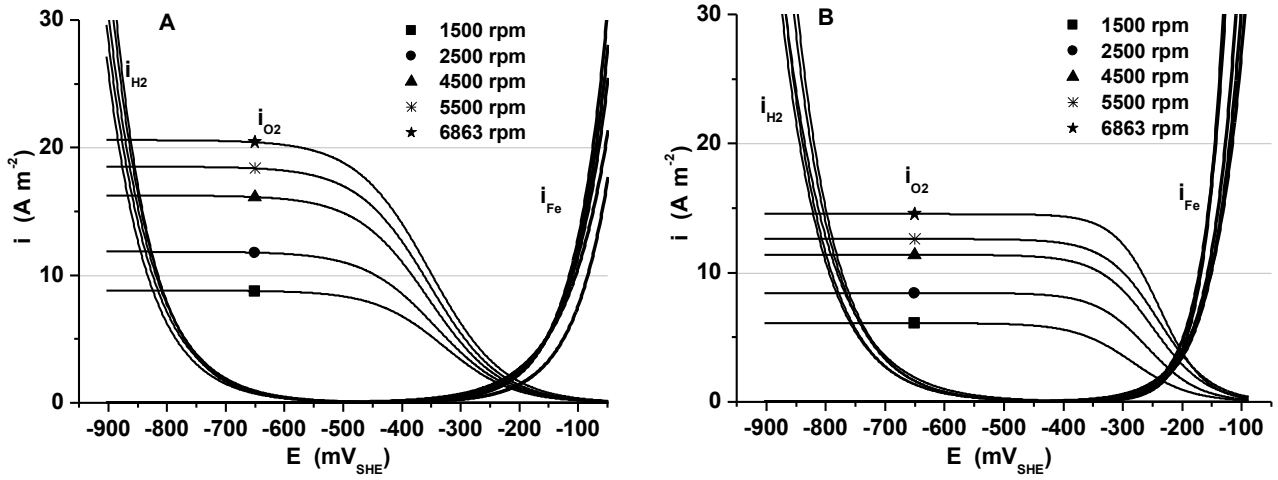

Figure 8. Rotation speed influence on partial polarization curves for anodic and cathodic sub-processes at concentrations of (A) 0.5 mol L^{-1} and (B) 2 mol L^{-1} LiBr solutions.

A good agreement between experimental and fitted values was observed validating the applicability of the mixed potential theory in corrosion studies of carbon steel electrodes immersed in concentrated solutions. Also, the Fig. 6 shows the graphical representation of the determination of the corrosion parameters according to the mixed potential theory in which the total anodic and cathodic current densities are balanced at E_{corr} value. Values of i_{corr} and E_{corr} are tabulated in Tables 2-4 for each test solution.

Figs. 7 and 8 shows paired plots of NaCl and LiBr solutions at 0.5 and 2 mol L^{-1}, respectively. Each single plot containing a family of synthesized partial polarization curves of carbon steel at different rotations rates of the electrode.

Fig. 9 shows a similar plot but for a mixture NaCl+LiBr at a total concentrations of 0.5 and 2 mol L^{-1}. It is very interesting to note that although the general shape and tendencies between polarizations plots for NaCl, LiBr and NaCl+LiBr mixture have minor discrepancies, the partial reactions between different salts exhibit interesting differences. For the iron oxidation kinetic, the first observation is that its current density is not significantly affected by an increase in rotation rate. However, it is noticeably affected by both the type and concentration of salt. In fact, the $i_{0,Fe}$ values for LiBr are between 1 to 3 order of magnitude higher than those corresponding to NaCl, the lowest differences are observed at a salt concentration of 2 mol L^{-1} (Tables 2 and 3).

Also the b_{Fe} values for LiBr are between 1.5 to 2 times higher than those corresponding to NaCl. The meaning of these differences is in reference to overpotentials and rate of change in the iron kinetics. The higher $i_{0,Fe}$ values means that it is easier to oxidize iron in LiBr than in NaCl solutions, or in other words a lower overpotential is needed in LiBr than in NaCl solutions to achieve similar values of oxidation current density. A higher b_{Fe} value for LiBr means a lower rate of iron oxidation in comparison with NaCl at similar potential values.

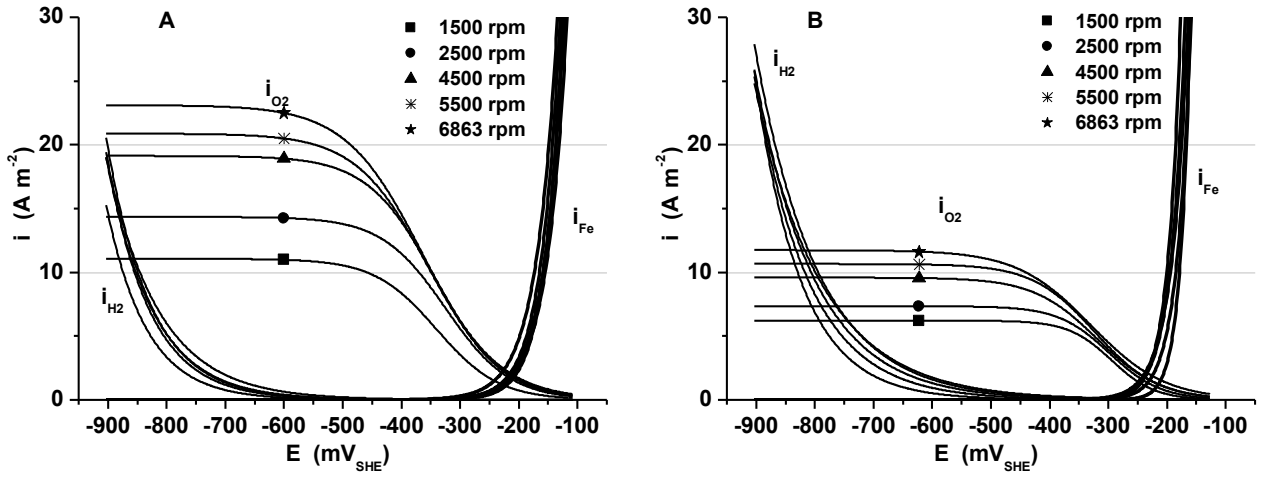

Figure 9. Rotation speed influence on partial polarization curves for anodic and cathodic subprocesses at concentrations of (A) 0.25 mol L^{-1} NaCl + 0.25 mol L^{-1} LiBr and (B) 1 mol L^{-1} NaCl + 1 mol L^{-1} LiBr solutions.

These effects are visualized in Figs. 7 and 8, as a slight anodic shift on the start potential for iron oxidation in NaCl in comparison with LiBr combined with a higher curve slope for NaCl in comparison with LiBr. For the hydrogen evolution reaction also the current density is not significantly affected by an increase in rotation rate, but is affected by both the type and concentration of salt, but in lower extent than iron oxidation reaction. Here, the $i_{0,H2}$ values for LiBr are between 1 to 2 order of magnitude higher than those corresponding to NaCl, but the b_{H2} values for LiBr are similar than those corresponding to NaCl. The comparative higher $i_{0,H2}$ value means that for hydrogen evolution a lower overpotential is needed for carbon steel in LiBr than in NaCl solutions to obtain similar values of current density. In Figs. 7 and 8 this is visualized as a slight cathodic shift on the start potential for a near null current density for hydrogen evolution in NaCl in comparison with LiBr. In contrast with iron oxidation and hydrogen evolution reactions, the current density for the ORR is significantly affected by rotation speed due to of mass transfer limitations for dissolved oxygen from the bulk to the metal surface. The $i_{l,O2}$ parameter representing this effect and evidenced as a planar plateau in i_{O2} curves (Figs. 7 and 8), which show an increasing trend in the absolute values with electrode rotation speed; for example $i_{l,O2}$ at 0.5 mol L^{-1} LiBr or NaCl changes from -9 A m^{-2} at 1500 rpm to -20 A m^{-2} at 6863 rpm. At higher concentrations these absolute values shows a slight decrease.

The kinetic parameters of steel in a mixture NaCl+LiBr at equal molar concentrations are shown in Table 4. The very similar iron oxidation kinetic parameter values observed between 0.25 mol L^{-1} NaCl + 0.25 mol L^{-1} LiBr and 0.5 mol L^{-1} NaCl, at larger concentrations present a notorious decreasing trend toward lower kinetic for the mixture NaCl+LiBr. This indicates that NaCl is significantly more influential on the iron kinetic than LiBr and also exists some sort of interaction between LiBr and NaCl that tend to block the iron kinetic rate. On the contrary, the hydrogen evolution reaction for the mixture NaCl+LiBr is more influenced by LiBr than NaCl but in this case the kinetic rates do not exhibit a decreasing trend at higher concentrations of NaCl+LiBr. For the ORR the kinetic parameters for NaCl+LiBr are very similar to NaCl and LiBr in respect to the decreasing trend in absolute values observed at increasing concentration.

3.5. Considerations for the mechanism of the oxygen reduction reaction

In the cathodic range extending approximately up to -600 mV_{SHE}, the partial ORR is controlled solely by oxygen mass transfer from the bulk up to the metal surface where there is a null concentration of oxygen. Accordingly, the i_{O2} in this range is only dependent of fluid-dynamics regime and transport properties of the electrolyte. A detailed theoretical analysis of this situation [13] is based on the steady-state convective-diffusion equation which is coupled with an expression for a velocity profile solution in cylindrical coordinates in addition with appropriate boundary conditions for the oxygen transport from the bulk up to a rotating disk surface at a fixed rotation speed. Expressing the oxygen flux rate solution at the surface in terms of the Faraday´s equivalence the Levich´s equation is obtained [9, 13, 35]:

$$i_{l,O2}=0.62nFC_{b,O2}D^{2/3}v^{-1/6}w^{1/2} \quad (11)$$

where, n is the number of exchanged electrons in the ORR, F is the Faraday constant (96485 C mol^{-1}), and w is the angular velocity of the disc electrode expressed in radian per second.

In all solutions tested, the $|i_{l,O2}|$ values were increasing with the rotation speed at a rate compatible with Eq. (11) as is showed in Fig. 10. The influence of increasing salt concentration is manifested as a curve downward displacement, which is explained in terms of the concentration dependence parameters $C_{b,O2}$, D and v values.

The inset figure in Fig. 10 shows the Levich plots $|i_{l,O2}|$ vs. $w^{1/2}$ for experimental data at different concentrations of NaCl, LiBr and NaCl+LiBr solutions. The experimental Levich slopes for both NaCl and LiBr solutions which are equivalent to the proportionality factor $S=|i_{l,O2}|/w^{1/2}$ present a deviation between 2 to 12% with respect to predicted S values ($0.62nFC_{b,O2}D^{2/3}v^{-1/6}$) of Table 1 assuming four exchanged electrons. This deviation increases up to 18% for mixed NaCl+LiBr solutions, which are attributed mainly to lower $C_{b,O2}$ experimental values.

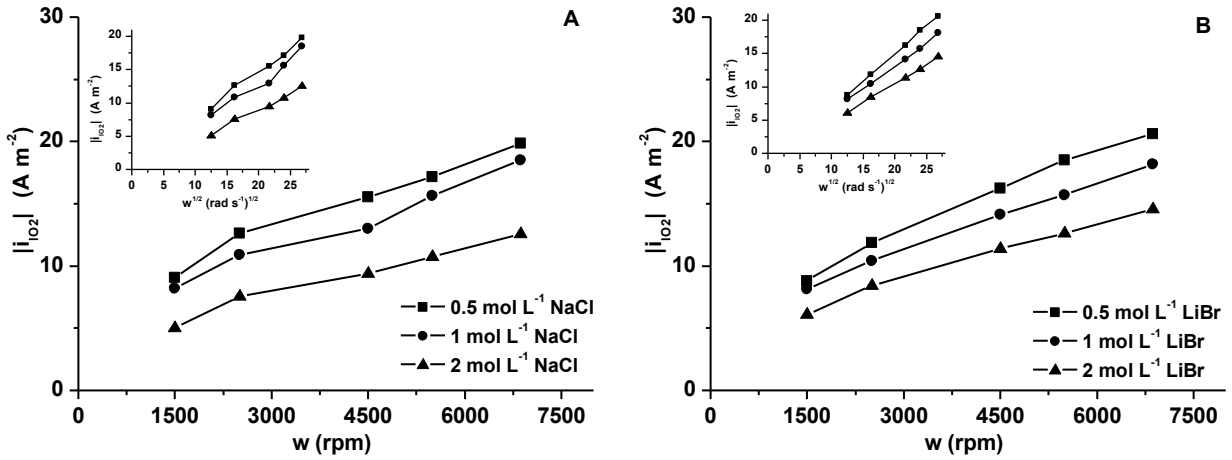

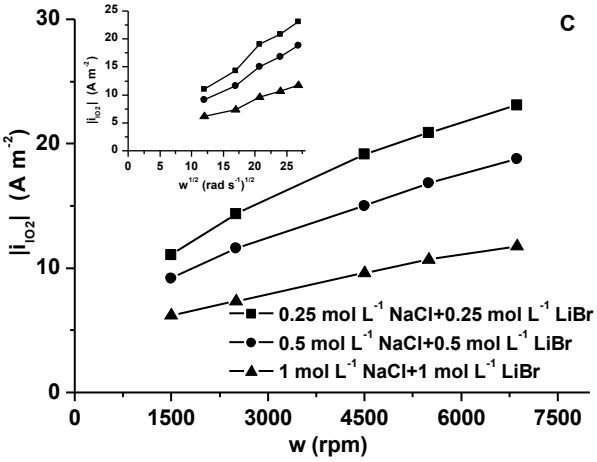

Figure 10. Influence of the rotation speed on the oxygen limiting current density for carbon steel electrodes in aerated (A) NaCl, (B) LiBr and (C) NaCl+LiBr solutions. Inset: Levich plot showing the $|i_{l,O2}|$ vs $w^{1/2}$.

The physical factors that influence dissolved oxygen are not only temperature, altitude and salinity, but also fluid dynamics conditions. Dismissing this deviation, the preceding information is an additional confirmation that the ORR is controlled by a mass transfer mechanism [36].

At potentials higher than -600 mV_{SHE} the oxygen concentration at the metal surface should be greater than zero, and the incidence of electron transfer reaction must become increasingly important up to a zone near the corrosion potential where the reaction should proceed with a pure charge transfer mechanism. In this respect, the factor $(1-i_{O2}/i_{l,O2})$ in Eq. (5) is a proportionality factor indicating the degree of incidence of the charge transfer reaction on the global ORR kinetics. From the determined numerical value for this factor, which is greater than 0.8 for all runs, it can be stated that at the E_{corr} potential the ORR reaction takes place through a nearly pure charge transfer mechanism.

3.6. Influence of salt concentration and rotation speed on the corrosion parameters

One important consequence of the variability described in section 3.4 is its impact on the intersection point between the polarization curves for iron oxidation and ORR which is nearly positioned at the E_{corr} value. Neglecting the influence of hydrogen evolution reaction, the absolute current density for iron oxidation becomes equal to ORR at this potential [2, 9, 13]. The influence of rotation speed and salt type and its concentration on the intersection point is described for E_{corr} and i_{corr} separately. At increasing rotation speed, the E_{corr} values do not change significantly by the exception for LiBr solutions where a slight anodic shift is observed. The same condition induces an increase in the i_{corr} values. At increasing NaCl solution concentration, the E_{corr} value is shifted toward more cathodic potentials and the i_{corr} presents a maximum value at 1 mol L^{-1} concentration. In contrast for LiBr solutions, the E_{corr} shift does not occur and the i_{corr} do not show an intermediate maximum value. Fig. 11 shows the corrosion rate versus the rotation speed at different concentrations of NaCl and LiBr in solution.

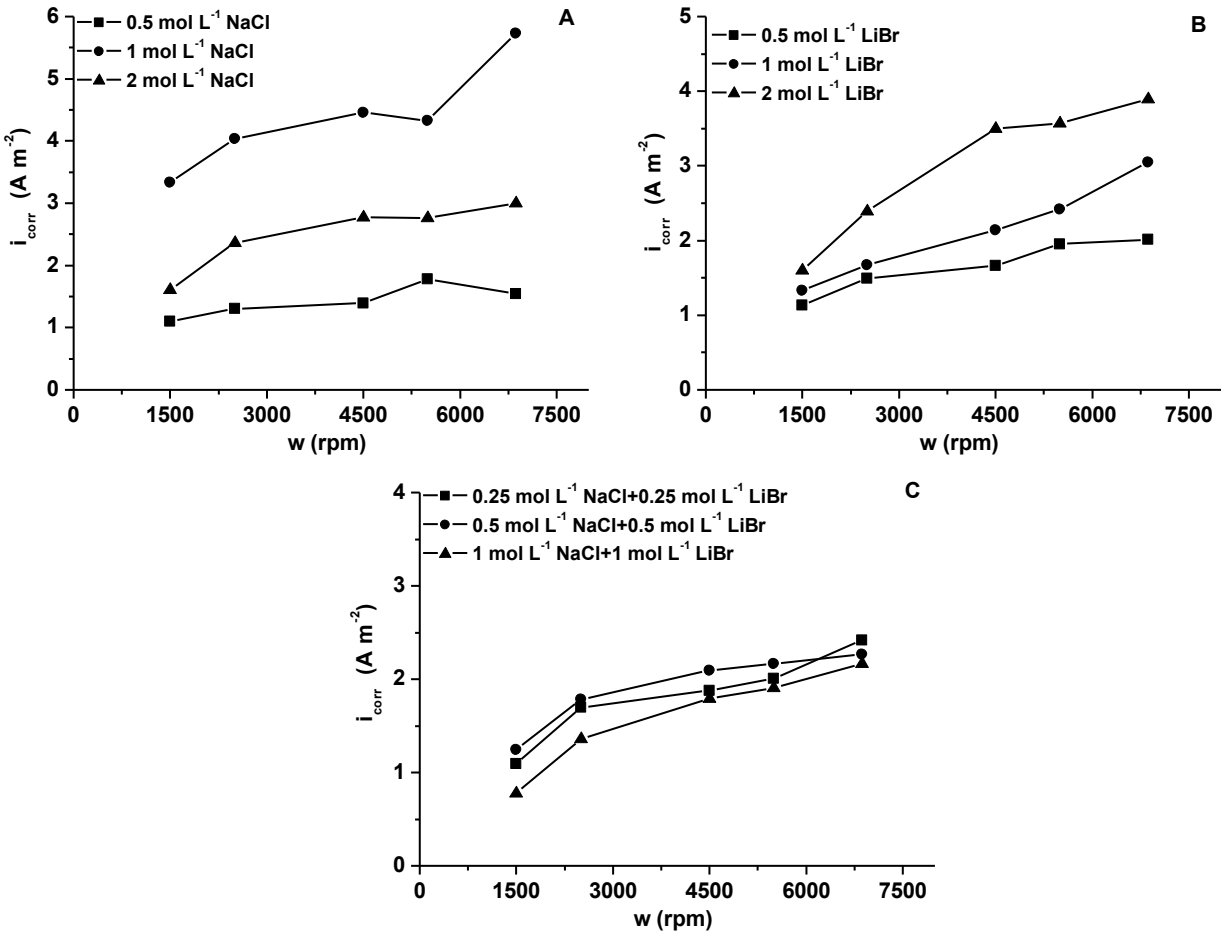

Figure 11. Influence of the rotation speed on the corrosion current density for carbon steel electrodes in aerated (A) NaCl, (B) LiBr and (C) NaCl+LiBr solution at total concentrations of 0.5, 1 and 2 mol L^{-1}.

For the case of the NaCl solutions (Fig. 11A), it is seen that for solutions 0.5 and 2 mol L^{-1} the corrosion rates tend to reach constant values at high rotation speeds, in contrast to the corrosion rates obtained in solutions 1 mol L^{-1} NaCl where the corrosion rates values *were continuously increasing* with the rotation speed. On the other hand, the influence of the NaCl concentration shows that the increase in corrosion rate up to 1 mol L^{-1} NaCl, is followed by an abrupt decrease at concentrated solutions of 2 mol L^{-1}. Then, the concentration of 1 mol L^{-1} NaCl can be considered as a threshold for the corrosion rate in NaCl solutions. This decrease can be attributed to a decrease in mass transfer of oxygen provoked by a combination of lower saturated dissolved oxygen concentration and higher viscosity that occur at high NaCl concentration conducting to obtain low corrosion rates [37]. Previous studies for the corrosion of carbon steel in solution with concentration lower than 1 mol L^{-1} NaCl are in agreement with the results obtained in this study [9]. For the case of the LiBr solution (Fig. 7B), the corrosion rates increase continuously with an increase in rotation speed. However, the corrosion rate variations with the concentration do not exhibit a concentration threshold value, as was observed in NaCl solutions. According to the results at concentrations larger than 1 mol L^{-1} the bromide anions reveal to be more aggressive than the chloride anions for the carbon steel corrosion process.

3.7. Morphological analysis

The morphological inspections of the corroded surface were made through images of samples with and without surface rust. Samples with rust were taken in a visual microscope immediately after a polarization curve measurement, whereas samples free of rust were taken in a SEM microscope after 10-minutes sonication in 5% acid citric solution.

Images taken with a visual microscope (Fig. 12A) shows that a fraction of the surface with oxide layer, exhibit a tail-like pattern that start from larger pits suggesting its pouring from growing pits.

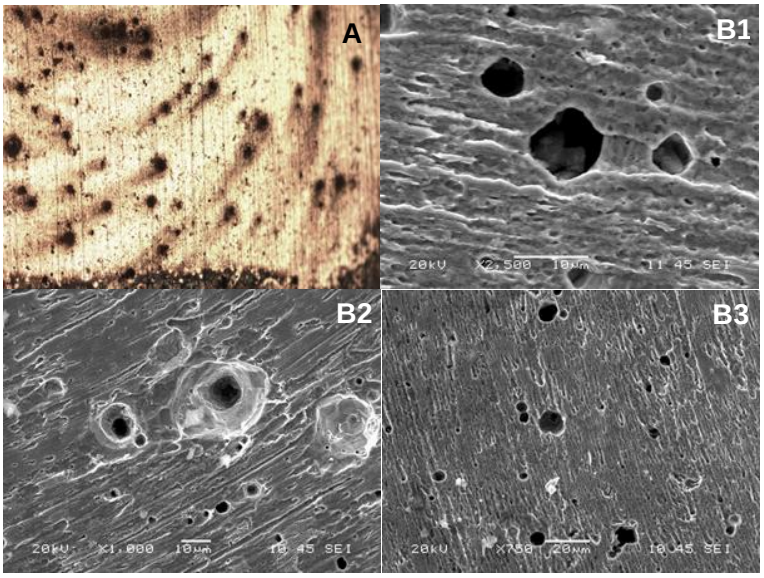

Figure 12. Images of the carbon steel electrodes after linear polarization experiments. (A) Images obtained with an optical microscope with 10X of magnitude, (B) Images obtained with a scanning electronic microscope (SEM), (B1) NaCl, (B2) LiBr and (B3) NaCl+LiBr solutions.

The SEM micrographs shows that the surface morphology contain two basic features, a concentrically circular grind lines left when polishing in a lathing machine and distributed cavities left by localized corrosion. Unlike pitting cavities formed in NaCl, which shows well delineated contours that not change with size (Fig. 12B1), cavities formed under LiBr solutions shows diffuse borders (Fig. 12B2). This indicates faster iron oxidation kinetics for LiBr which agrees with kinetic parameter description given in section 3.4. In this respect it is important to point out that because of the significant higher $i_{0,Fe}$ parameter for LiBr than NaCl, the LiBr kinetics will be faster than that of the NaCl provided that the iron overpotential is not significant. This is because the lower b_{Fe} value for NaCl means faster rate of kinetic increase than LiBr, and therefore at sufficiently high overpotential the iron kinetics will be becomes higher than that of the LiBr despite the higher $i_{0,Fe}$ value for LiBr. On the other hand, the pits observed on the surface exposed to the mixture NaCl+LiBr (Fig. 12B3) show similar shapes to the pits observed in solutions of NaCl. These observations for the mixture NaCl+LiBr are in agreement with the kinetic parameters $i_{0,Fe}$ and b_{Fe}, which shows values more close to the kinetic parameters obtained for NaCl than that obtained for LiBr solutions.

4. CONCLUSIONS

In this work the corrosion behavior of carbon steel AISI 1020 in LiBr in comparison with NaCl solutions were studied from polarization curve under a combination of different salt concentrations and rotation speeds of the electrode. The experimental potential-current density data were expressed in terms of a kinetic model in which hydrogen evolution and oxygen reduction reactions are the cathodic counterparts of the iron oxidation reaction.

Despite of the close similarities and tendencies observed for carbon steel corrosion with rotation speed and salt concentration between LiBr and NaCl, distinct differences were found in the kinetic for partial electrochemical reactions.

1) For iron oxidation, the $i_{0,Fe}$ values for LiBr are between 1 to 3 orders of magnitude higher than those corresponding to NaCl. Also the b_{Fe} values for LiBr are between 1.5 to 2 times higher than those corresponding to NaCl. The impact of these differences is represented in the rate of iron oxidation which is higher in LiBr than in NaCl, which coincides with morphological attributes of the pits observed under LiBr which shows pits with more extensive damage in comparison with those formed in NaCl.

2) For hydrogen evolution the $i_{0,Fe}$ values for LiBr are between 1 to 2 order of magnitude higher than those corresponding to NaCl, but the b_{H2} values for LiBr are similar than those corresponding to NaCl. The effect of this is in a lower overpotential needed for carbon steel in LiBr than in NaCl solutions to obtain similar values of current density.

3) For the oxygen reduction reaction the minor kinetic differences observed between NaCl and LiBr are attributed to transport properties of the electrolyte. In this case the $i_{l,O2}$ values are the most influential kinetic parameter and its variability is in full agreement with theoretical predictions.

The kinetic parameters of steel in a mixture NaCl+LiBr at equal molar concentrations present a degree of asymmetry. This means that while for iron kinetics, NaCl is significantly more influential than LiBr, for the hydrogen evolution reaction it is just the opposite. For the oxygen reduction reaction the kinetic parameters are very similar to NaCl and LiBr in respect to the decreasing trend in absolute values observed at increasing concentration.

ACKNOWLEDGEMENTS

The authors gratefully the financial support through of CICITEM and the project MECESUP-ANT0709: Fortalecimiento del Programa de Doctorado en Ingeniería de Procesos de Minerales carried out at the Universidad de Antofagasta, Chile.

References

1. L. L. Shreir, R. A. Jarman and G. T. Burnstein, *Corrosion*, Vol. 1, Butterworth Heinemann, Great Britain (2000)
2. P. Marcus and F. Mansfeld, *Analytical Methods in Corrosion Science and Engineering*, CRC Press Taylor & Francis Group, Florida (2006)
3. Y. Kaita, *Int. J. Refrig.*, 24 (2001) 374
4. H. T. Chua, H. K. Toh, A. Malek, K. C. Ng and K. Srinivasan, *Int. J. Refrig.*, 23 (2000) 412

5. R.H. Perry, D.W. Green, *Perrys' Chemical Engineers' Handbook*, McGraw-Hill, New York (1997)
6. L. Li, C. Wang and H. Lu, *Electrochim. Acta*, 104 (2013) 295
7. M. A. C. de Castro and B. E. Wilde, *Corros. Sci.*, 19 (1979) 923
8. K. Yazdanfar, X. Zhang, P. G. Keech, D. W. Shoesmith and J. C. Wren, *Corros. Sci.*, 52 (2010) 1297
9. L. Cáceres, T. Vargas and M. Parra, *Electrochim. Acta*, 54 (2009) 7435
10. B.W.A. Sherar, P. G. Keech and D. W. Shoesmith, *Corros. Sci.*, 53 (2011) 3636
11. K. Tanno, M. Itoh, T. Takayashi, H. Yashiro and N. Kumagai, *Corros. Sci.*, 34 (1993) 1441
12. M. T. Montañés, R. Sánchez-Tovar, J. García-Antón and V. Pérez-Herranz, *Corros. Sci.*, 51 (2009) 2733
13. A. J. Bard and L. R. Faulkner, *Electrochemical methods: Fundamentals and Applications*, John Wiley & Sons, Inc., New York (2001)
14. H. S. Klapper, D. Laverde and C. Vasquez, *Corros. Sci.*, 50 (2008) 2718
15. E. McCafferty, *Corros. Sci.*, 47 (2005) 3202
16. Q. Qu, R. Yuan, L. Li, Y. He, J. Luo, L. Wang, H. Xu, Y. Gao, Y. Song and Z. Ding, *Int. J. Electrochem. Sci.*, 8 (2013) 11625
17. J. Sudagar, G. Bi, Z. Jiang, G. Li, Q. Jiang and J. Lian, *Int. J. Electrochem. Sci.*, 6 (2011) 2767
18. H. J. Flitt and D. P. Schweinsberg, *Corros. Sci.*, 47 (2005) 3034
19. A. Lecante, F. Robert, M. Lebrini and C. Roos, *Int. J. Electrochem. Sci.*, 6 (2011) 5249
20. L. Cáceres, T. Vargas and L. Herrera, *Corros. Sci.*, 49 (2007) 3168
21. C. Wagner and W. Traud, *Z. F. Elektroch. Bd.*, 44 (1938) 391
22. Y. S. Liu, Y. F. Hu, Q. C. Hao, X. M. Zhang, Z. C. Liu and J. G. Li, *J. Chem. Eng. Data*, 54 (2009) 739
23. C. S. Ho, L. K. Ju, R. F. Baddour and D. I. C. Wang, *Chem. Eng. Sci.*, 43 (1988) 3093
24. J. M. Wimby and T. S. Berntsson, *J. Chem. Eng. Data*, 39 (1994) 68
25. C. R. Wilke and P. Chang, *AIChE J.*, 1 (1955) 264
26. T. N. Andersen, B. S. Dandapani and J. M. Berry, *J. Electroanal. Chem.*, 357 (1993) 77
27. A. Davydov, K. V. Rybalka, L. A. Beketaeva, G. R. Engelhardt, P. Jayaweera and D. D. Macdonald, *Corros. Sci.*, 47 (2005) 195
28. A. Frumkin, V. Korshunov and I. Bagazkaya, *Electrochim. Acta*, 15 (1970) 289
29. J. Bockris, A. Reddy and M. Gamboa-Adelco, *Electrochemistry in Materials Science, in: Modern Electrochemistry 2B*, Kluwer Academic/Plenum Pub., New York (1998)
30. M. B. Ives, Y. C. Lu and J. L. Juo, *Corros. Sci.*, 32 (991) 91
31. L. Cáceres, T. Vargas and L. Herrera, *Corros. Sci.*, 51 (2009) 971
32. Y. Miyata and S. Asakura, *Corros. Sci.*, 44 (2002) 589
33. J. Zeng, S. Liao, J. Y. Lee and Z. Liang, *Int. J. Hydrogen Energ.*, 35 (2010) 942
34. H. S. Wroblowa and S. B. Qaderi, *J. Electroanal. Chem.*, 279 (1990) 231
35. N. Le Bozec, C. Compère, M. L'Her, A. Laouenan, D. Costa and P. Marcus, *Corros. Sci.*, 43 (2001) 765
36. M. F. Li, L. W. Liao, D. F. Yuan, D. Mei and Y. X. Chen, *Electrochim. Acta*, 110 (2013) 780
37. J. Han, J. W. Carey and J. Zhang, *J. Appl. Electrochem.*, 41 (2011) 741